

# A mathematical model of MHD nanofluid flow having gyrotactic microorganisms with thermal radiation and chemical reaction effects

M. M. Bhatti<sup>1</sup> · S. R. Mishra<sup>2</sup> · T. Abbas<sup>3</sup> · M. M. Rashidi<sup>4</sup>

Received: 11 August 2016 / Accepted: 25 November 2016 / Published online: 10 December 2016  
© The Natural Computing Applications Forum 2016

**Abstract** In this article, we have examined three-dimensional unsteady MHD boundary layer flow of viscous nanofluid having gyrotactic microorganisms through a stretching porous cylinder. Simultaneous effects of nonlinear thermal radiation and chemical reaction are taken into account. Moreover, the effects of velocity slip and thermal slip are also considered. The governing flow problem is modelled by means of similarity transformation variables with their relevant boundary conditions. The obtained reduced highly nonlinear coupled ordinary differential equations are solved numerically by means of nonlinear shooting technique. The effects of all the governing parameters are discussed for velocity profile, temperature profile, nanoparticle concentration profile and motile microorganisms' density function presented with the help of tables and graphs. The numerical comparison is also presented with the existing published results as a special case of our study. It is found that velocity of the fluid diminishes for large values of magnetic parameter and porosity parameter. Radiation effects show an increment in the temperature profile, whereas thermal slip parameter shows converse effect. Furthermore, it is also observed that

chemical reaction parameter significantly enhances the nanoparticle concentration profile. The present study is also applicable in bio-nano-polymer process and in different industrial process.

**Keywords** Magnetic field · Chemical reaction · Nanofluid · Numerical solution · Gyrotactic microorganisms

## List of symbols

$\bar{u}, \bar{v}, \bar{w}$	Velocity components
$\bar{r}, \bar{z}$	Cylindrical coordinate
$Re$	Reynolds number
$\bar{t}$	Time
$\bar{C}$	Nanoparticle volume fraction
$\bar{P}$	Pressure
$F_w$	Suction/injection parameter
$\bar{T}_\infty$	Atmosphere temperature
$\bar{C}_\infty$	Atmosphere concentration
$\bar{T}_w$	Surface temperature
$N_t$	Thermophoresis parameter
$N_b$	Brownian motion parameter
$N_1$	Velocity slip parameter
$\bar{n}_w$	Surface density of motile-organism
$\bar{k}_p$	Permeability of porous medium
$\bar{t}$	Time
$J$	Heat flux of microorganisms
$a_0 (>0)$	Constant
$c_F$	Forchheimer coefficient
$Q_0$	Heat source/sink
$\bar{D}_1$	Thermal slip factor
$D_{\bar{T}}$	Thermophoretic diffusion coefficient
$\bar{n}$	Density of motile microorganisms
$\bar{b}$	Chemotaxis constant

✉ M. M. Bhatti  
mubashirme@yahoo.com; muhammad09@shu.edu.cn

<sup>1</sup> Shanghai Institute of Applied Mathematics and Mechanics, Shanghai University, Shanghai 200072, China

<sup>2</sup> Department of Mathematics, Siksha 'O' Anusandhan University, Khandagiri, Bhubaneswar, Odisha 751030, India

<sup>3</sup> Department of Mathematics, Quaid-I-Azam University, Islamabad 44000, Pakistan

<sup>4</sup> Shanghai Key Lab of Vehicle Aerodynamics and Vehicle Thermal Management Systems, Tongji University, Shanghai 201804, China

$W_c$	Maximum cell swimming speed
$S$	Unsteady parameter
$D_B$	Brownian diffusion coefficient
$D_{\bar{n}}$	A micro-organism diffusivity
$Pr$	Prandtl number
$Sc$	Schmidt number
$Sb$	Bio-convection Schmidt number
$Pe$	Peclet number
$k_f$	Forchheimer number
$M$	Magnetic parameter
$R_d$	Thermal radiation parameter
$H_S$	Heat source/sink parameter
$q_w$	Surface heat flux
$q_M$	Surface mass flux
$q_N$	Motile surface microorganism flux
$k'$	Mean absorption coefficient
$C_{F\bar{x}}$	Skin friction coefficient
$Nu_{\bar{x}}$	Nusselt number
$Sh_{\bar{x}}$	Sherwood number
$N_{n\bar{x}}$	Density number of motile microorganisms

### Greek symbols

$\bar{\beta}$	Contraction expansion strength
$\bar{\alpha}_m$	Thermal conductivity
$(\rho c)_f$	Heat capacity of the fluid
$(\rho c)_p$	Heat capacity of nanoparticle
$\sigma$	Electrical conductivity
$\mu$	Viscosity of nanofluid
$\theta$	Temperature profile
$\phi$	Nanoparticle concentration profile
$\Phi$	Motile microorganism density profile
$\bar{\sigma}$	Stefan–Boltzmann constant
$\beta$	Velocity slip
$\tau_w$	Shear stress
$\rho_p$	Density of nanoparticles
$\sigma$	Electrical conductivity
$\beta_T$	Thermal slip
$\rho$	Density
$\nu$	Kinematic viscosity
$\gamma$	Chemical reaction parameter

## 1 Introduction

The flow through a stretching surface grabs the attention of researchers due to its huge number of applications in the extrusion of plastic sheets, aerodynamics, production of paper, condensation process of boundary layer liquid film and glass blowing. Thomas and Yang [1] presented numerous applications for stretching wedges, sheets, nano-bio-polymers and in differential geometrical aspects. Stasiak et al. [2] addressed in detail the effects of stretching on

the physical features for bio-polymer cylindrical coatings. Bachok and Ishak [3] investigated the heat flux with heat transfer through a stretching cylinder. Stretching or contracting has a significant importance which is critical for the accomplishment of polymer products from a macroscopic to a nanoscale level. The boundary layer flow on a moving stretching surface was first considered by Sakiadis [4]. Further, this concept of stretching surface was extended by Crane [5]. In his paper, he studied stretching sheet with linearly varying surface speed for steady two-dimensional flow. Moreover, the work of Crane [5] was extended by Datta et al. [6] and Chen and Char [7]. They have studied the heat and mass transfer analysis of different physical situations. Bhatti et al. [8] studied numerically the fluid flow through a porous shrinking sheet using successive linearisation method and Chebyshev spectral collocation method. Bhatti et al. [9] again analysed the effects magnetohydrodynamics over a permeable shrinking/stretching sheet through a porous medium with heat transfer.

During the past two decades, an important development in thermal engineering and material science has been that of nanofluids. Nanofluids contain very small nanoparticles ( $d \leq 50$  nm) in base fluids, i.e. water, ethylene glycol, oil, whereas nanoparticle is made up of oxides and metals such as nitride ceramics (AlN, SiN), semiconductors (SiC) and metals (Ag, Cu, Au). The suspension of nanoparticles in a base fluid can help to enhance markedly the thermal conductivity of the fluid, heat transfer proficiency and fluid flow characteristics, etc. This has implications in a treatment of cancer during thermal therapy, aerospace, power generation, micromanufacturing and various medical applications [10–12].

Bio-convection is associated with a macroscopic motion of convecting fluid influenced by density gradients due to hydrodynamic propulsion such as swimming of motile microorganism. The suspension of microorganism, i.e. bacteria and algae into a base fluid, i.e. water produces the process of bio-convection. This process is directly oriented swimming and typically through a naturally or imposed present stimulus such as magnetic field, gravity, chemical concentration (oxygen) and light. The density of a microorganism in inclined is higher as compared to a free stream fluid. Hence, an unstable density profile has been observed with a consecutive upending of a fluid against gravity [13]. To survive and remain active for most of the microorganism, the base fluid is considered as water and it is supposed to be that the addition of nanoparticles will remain secure and do not aggregate for few weeks [14]. Due to dilute suspension, bio-convection takes place since nanoparticle will enhance the suspension's viscosity and viscosity will govern the bio-convection instability [15]. Xu

and Pop [16] studied the mixed convection nanofluid flow having gyrotactic microorganism through a stretching surface. Aziz et al. [17] examined the natural bio-convection nanofluid boundary layer flow and found that the bio-convection parameters create an effect on the motile microorganism, heat and mass transfer. Bio-convection plays a significant role in bio-microsystems for the propagation of mass augmentation and different microfluidics devices, i.e. bacteria powered micromixers [18]. Furthermore, nanofluids with bio-convection can be found in the synthesis of drug delivery systems (pharmacological agents) [19, 20]. Microorganism is employed to enhance different desirable medical features, i.e. biocompatibility, DNA (gene therapy), bioavailability, protein deliverability and encapsulation, whereas it is also helpful to improve a biodegradable nanomaterials. Nowadays, the manufacturer of bio-nanopolymers introduced various kinds of drugs that can achieve control release which is very helpful to enhance the influence of therapeutic in patients. For example, polylactic acid, polycaprolactone, chitosan–gelatin, poly alkyl cyanoacrylate, poly (lactic-co-glycolic acid) and polyhydroxylalkanoates.

Heat transfer with thermal radiation plays a significant influence in the establishment of high temperature. The different technological process performs at high temperature, and an excellent knowledge of radiative heat transfer plays a worthy role to manipulate the apparatus. In different applications depending on geometry as well as surface properties, the transfer of radiation is similar to a convective heat transfer. In the study of radiative heat transfer fluid flow, a few complexities arise. Firstly, when the radiative heat transfer arises, the radiation diffused in the periphery of a system as well as at system restrictions. Hence, the prophecy of a fluid amalgamation is a complicated chore. Secondly, the thermal radiation term that arises in the energy equation makes the equation nonlinear. Thirdly, the coefficient of amalgamation of alluring fluids markedly depends on wavelength. Due to such kinds of complexities, the influence of energy on convecting fluid flow has been analysed with rationally simplified models. For instance, the radiation effect on heat transfer in electrically conducting fluid at a stretching surface with uniform free stream was examined by Eldahab and Aziz [21]. Cortell [22] studied the effects of viscous dissipation and work done by deformation on MHD flow and heat transfer of a viscoelastic fluid over a stretching sheet and also he [23] also observed the radiation effect on thermal boundary layer. Few more pertinent studies can be found from Refs. [24–26].

On the other hand, heat and mass transfer under the effects of chemical reaction has significant importance in many practical applications in science and engineering such as chemical engineering process, transfer of energy in a wet cooling tower and evaporation at the surface of water body.

Anjalidevi and Kandasamy [27] studied the simultaneous effects of chemical reaction with and mass transfer through the semi-infinite horizontal plate. Hayat et al. [28] addressed the heat and mass transfer with combine effects of radiation and chemical reaction on three-dimensional boundary layer flow of a second-grade nanofluids through a stretching surface. Abel et al. [29] examined the effects of variable thermal conductivity and buoyancy on magnetohydrodynamics boundary layer flow of a power-law fluid in the presence of heat source through a stretching sheet. Various authors [30–32] have examined different problems by considering nanofluid, thermal radiation, chemical reaction, magnetic field and viscous dissipation in various geometrical aspects.

The study of applied magnetic field also plays a prominent role in heat and mass transfer, controlling momentum in boundary layer nanofluid flow through a shrinking/stretching surface. Furthermore, magnetohydrodynamics (MHD) is applicable in various engineering applications such as cooling of the nuclear reactor, electromagnetic casting and plasma confinement. Moreover, in microfluidics problems, magnetohydrodynamics is helpful to create non-pulsating and continuous flow in the design of a complex microchannel. In biomedical engineering, magnetohydrodynamics is applicable for magnetic drug targeting in cancer diseases. Ishak et al. [33] investigated MHD effects on flow and heat transfer over a stretching cylinder. The slip condition plays an important role in shear skin and effect of hysteresis. It also arises in hydrophobic surfaces, particularly in, microfluidics. The effect of partial slip with MHD and chemically solute transfer over a stretching cylinder is studied by Mukhopadhyay [34]. The unsteady laminar flow of a viscous incompressible and electrically conducting fluid over a continuously stretching surface in the presence of magnetic field was investigated by Ishak [35]. Pop and Na [36] considered a note on MHD flow over a stretching permeable surface. Khan et al. [37] studied the viscoelastic MHD flow heat and mass transfer over a porous stretching sheet with the dissipation of energy and stress work.

The study of flow through a porous medium is also very important in engineering and industrial process. A porous media is a material having pores, i.e. oxides and metals, whereas these pores are covered with a fluid. Such type of flow has two main benefits, as its area of dissipation is higher as compared to conventional fins that improve the heat convection. Moreover, the regular motion of a fluid along the whole individual beads blends the fluid effectively [38]. According to some recent studies, it is found that nanofluid flow through a porous media reveals improved thermal properties, i.e. convective heat transfer coefficients as compared with a base material and higher thermal conductivity [39]. Therefore, a porous media having nanoparticles plays a vital role in the enhancement

of heat transfer and this mechanism is very important from an application and theoretical point of view. Such kinds of flow can be observed infiltration, oil flow, heat exchangers, drying process and geothermal systems [40]. Particularly, nanofluid flow through a porous media has many in thermal engineering such as favourable to improve the thermal properties of lubricants and oil [41] electronic cooling equipment and vehicle cooling.

Motivated from the above discussion, the aim of present study is to present a mathematical model of MHD viscous nanofluid having gyrotactic microorganism under the effects of thermal radiation and chemical reaction through a porous stretching cylinder. Simultaneous effects thermal slip and velocity slip are also taken into account in the presence of heat source/sink. For an excellent fabrication of bio-nano-materials, physio-mathematical and numerical simulation has played a significant role. This is a strong motivation for the present study. Numerical computation has been employed using shooting method to obtain the solution for the governing nonlinear highly coupled differential equations. The effects of all the governing parameters are discussed for velocity, temperature, nanoparticle concentration and motile microorganism density profile. Moreover, the expression for skin friction coefficient, Nusselt number, Sherwood number and motile microorganism density number is presented with the help of tables. The numerical comparison is also presented with the existing published results. This paper is organised in the following way; after the introduction and background in Sect. 1. Section 2 describes the mathematical formulation, while Sect. 4 deals with the solution methodology. Finally, Sect. 5 is devoted numerical and graphical results of all the physical parameters.

## 2 Mathematical formulation

Let us assume the unsteady forced nanofluid bio-convection flow that comprises of gyrotactic microorganism and nanoparticles through an infinite stretching cylinder. The diameter of a cylinder is considered a time function with unsteady radius, i.e.

$$\tilde{a} = a_0 \sqrt{1 - \tilde{\beta} \tilde{t}}, \quad (1)$$

where  $\tilde{\beta}$  is the contraction expansion strength,  $\tilde{t}$  is the time, and  $a_0 (>0)$  is a constant. The nanoparticles fraction on the atmosphere is supposed to follow the passively control modelled presented by Bashir et al. [44], whereas the temperature distribution and nanoparticles concentration on an atmosphere are considered as  $\bar{C}_\infty$  and  $\bar{T}_\infty$ , respectively. It is important to note that microorganisms can only live in water. For this purpose, we have considered the base fluid as a water (Fig. 1).

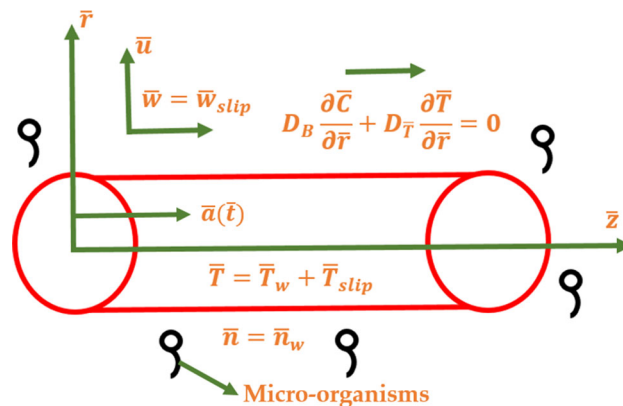


Fig. 1 Geometry of the problem

Using these assumptions and following Bashir et al. [44], the governing equations of continuity conservation of mass, thermal energy, nanoparticle concentration and microorganism concentration can be written as [44]

$$\nabla \cdot \bar{v} = 0, \quad (2)$$

$$\frac{\partial \bar{v}}{\partial \tilde{t}} + (\bar{v} \cdot \nabla) \bar{v} = -\frac{1}{\rho} \nabla \bar{P} + \nu \nabla^2 \bar{v} - \sigma B_0^2 \bar{v} - \frac{\mu}{\rho k_p} \bar{v} - \frac{c_F}{k_p^{1/2}} \bar{v}^2, \quad (3)$$

$$\frac{\partial \bar{T}}{\partial \tilde{t}} + \bar{v} \cdot \nabla \bar{T} = \bar{\alpha}_m \nabla^2 \bar{T} + \tau \left[ D_B \nabla \bar{T} \cdot \nabla \bar{C} + \frac{D_T}{T_\infty} \nabla \bar{T} \cdot \nabla \bar{T} \right] - \frac{1}{(\rho c)_p} \frac{\partial \bar{Q}_R}{\partial \tilde{r}} + \frac{Q_0 (\bar{T} - \bar{T}_\infty)}{(\rho c)_p}, \quad (4)$$

$$\frac{\partial \bar{C}}{\partial \tilde{t}} + \bar{v} \cdot \nabla \bar{C} = D_B \nabla^2 \bar{C} + \frac{\tau D_T}{T_\infty} \nabla^2 \bar{T} - k_1 (\bar{C}_w - \bar{C}_\infty), \quad (5)$$

$$\frac{\partial \bar{n}}{\partial \tilde{t}} + \nabla \cdot \bar{J} = 0. \quad (6)$$

The nonlinear radiative heat flux can be written as

$$\bar{Q}_r = -\frac{4\bar{\sigma}}{3k'} \frac{\partial \bar{T}^4}{\partial \tilde{r}} = -\frac{16\bar{\sigma} \bar{T}^3}{3k'} \frac{\partial \bar{T}}{\partial \tilde{r}}, \quad (7)$$

where  $\bar{v} = [\bar{u}, \bar{v}, \bar{w}]$  is the velocity components,  $\bar{P}$  is the pressure,  $\bar{C}$  is the nanoparticle volume fraction,  $\bar{n}$  is the density of motile microorganisms,  $\nu$  is a kinematic viscosity of a suspension of microorganism and nanofluid,  $\rho$  is the density,  $\bar{\alpha}_m$  is the thermal conductivity,  $\tau = (\rho c)_p / (\rho c)_f$  is parameter in which  $(\rho c)_f$  and  $(\rho c)_p$  is the heat capacity of the fluid and nanoparticle, respectively,  $\sigma$  is the electrical conductivity,  $D_B$  is a Brownian diffusion coefficient,  $D_T$  is a thermophoretic diffusion coefficient,  $J$  is a heat flux of microorganisms due to a convection of fluid, diffusion and self-propelled swimming are described as  $J = \bar{n} \bar{v} + \bar{n} \hat{v} - D_{\bar{n}} \nabla \bar{n}$ , where  $\hat{v} = \left\{ \frac{\bar{b} W_c}{\bar{c}_\infty} \right\} \nabla \bar{C}$  is a velocity vector associated

with swimming of cell in nanofluids,  $D_{\bar{n}}$  is a microorganism diffusivity,  $\bar{b}$  is a chemotaxis constant, and  $W_c$  is maximum cell swimming speed. We have considered cylindrical coordinates  $(\bar{r}, \bar{z})$  in radial and axial directions. Taking the approximation of boundary layer flow under the assumptions of axisymmetric flow, neglecting the velocity components of azimuthal and order of a magnitude analysis, the governing equations reduce to the following form [44]

$$\frac{\partial \bar{u}}{\partial \bar{r}} + \frac{\partial \bar{w}}{\partial \bar{z}} + \frac{\bar{u}}{\bar{r}} = 0, \tag{8}$$

$$\frac{\partial \bar{u}}{\partial \bar{r}} + \bar{u} \frac{\partial \bar{u}}{\partial \bar{r}} + \bar{w} \frac{\partial \bar{u}}{\partial \bar{z}} = -\frac{1}{\rho} \frac{\partial \bar{P}}{\partial \bar{r}} + \nu \left[ \frac{\partial^2 \bar{u}}{\partial \bar{r}^2} + \frac{\partial^2 \bar{u}}{\partial \bar{z}^2} + \frac{1}{\bar{r}} \frac{\partial \bar{u}}{\partial \bar{r}} - \frac{\bar{u}}{\bar{r}^2} \right], \tag{9}$$

$$\begin{aligned} \frac{\partial \bar{w}}{\partial \bar{r}} + \bar{u} \frac{\partial \bar{w}}{\partial \bar{r}} + \bar{w} \frac{\partial \bar{w}}{\partial \bar{z}} &= -\frac{1}{\rho} \frac{\partial \bar{P}}{\partial \bar{z}} + \nu \left[ \frac{\partial^2 \bar{w}}{\partial \bar{r}^2} + \frac{\partial^2 \bar{w}}{\partial \bar{z}^2} + \frac{1}{\bar{r}} \frac{\partial \bar{w}}{\partial \bar{r}} \right] \\ &\quad - \sigma B_0^2 \bar{w} - \frac{\mu}{\rho k_p} \bar{w} - \frac{c_F}{k_p^{1/2}} \bar{w}^2, \end{aligned} \tag{10}$$

$$\begin{aligned} \frac{\partial \bar{T}}{\partial \bar{r}} + \bar{u} \frac{\partial \bar{T}}{\partial \bar{r}} + \bar{w} \frac{\partial \bar{T}}{\partial \bar{z}} &= \bar{\alpha}_m \left[ \frac{\partial^2 \bar{T}}{\partial \bar{r}^2} + \frac{\partial^2 \bar{T}}{\partial \bar{z}^2} + \frac{1}{\bar{r}} \frac{\partial \bar{T}}{\partial \bar{r}} \right] \\ &\quad + \tau D_B \left[ \frac{\partial \bar{T}}{\partial \bar{r}} \frac{\partial \bar{C}}{\partial \bar{r}} + \frac{\partial \bar{T}}{\partial \bar{z}} \frac{\partial \bar{C}}{\partial \bar{z}} \right] \\ &\quad + \frac{\tau D_T}{T_\infty} \left[ \left( \frac{\partial \bar{T}}{\partial \bar{r}} \right)^2 + \left( \frac{\partial \bar{T}}{\partial \bar{z}} \right)^2 \right] \\ &\quad + \frac{16\sigma \bar{T}^3}{3k'} \frac{\partial^2 \bar{T}}{\partial \bar{r}^2} + \frac{Q_0(\bar{T} - \bar{T}_\infty)}{(\rho c)}, \end{aligned} \tag{11}$$

$$\begin{aligned} \frac{\partial \bar{C}}{\partial \bar{r}} + \bar{u} \frac{\partial \bar{C}}{\partial \bar{r}} + \bar{w} \frac{\partial \bar{C}}{\partial \bar{z}} &= D_B \left[ \frac{\partial^2 \bar{C}}{\partial \bar{r}^2} + \frac{\partial^2 \bar{C}}{\partial \bar{z}^2} + \frac{1}{\bar{r}} \frac{\partial \bar{C}}{\partial \bar{r}} \right] \\ &\quad + \frac{D_T}{T_\infty} \left[ \frac{\partial^2 \bar{T}}{\partial \bar{r}^2} + \frac{\partial^2 \bar{T}}{\partial \bar{z}^2} + \frac{1}{\bar{r}} \frac{\partial \bar{w}}{\partial \bar{r}} \right] \\ &\quad - k_1(\bar{C}_w - \bar{C}_\infty), \end{aligned} \tag{12}$$

$$\begin{aligned} \frac{\partial \bar{n}}{\partial \bar{r}} + \bar{u} \frac{\partial \bar{n}}{\partial \bar{r}} + \bar{w} \frac{\partial \bar{n}}{\partial \bar{z}} &= \frac{\bar{b}W_c}{C_\infty} \left[ \frac{\partial}{\partial \bar{r}} \left\{ \bar{n} \frac{\partial \bar{C}}{\partial \bar{r}} \right\} + \frac{\partial}{\partial \bar{z}} \left\{ \bar{n} \frac{\partial \bar{C}}{\partial \bar{z}} \right\} \right] \\ &\quad + D_{\bar{n}} \left[ \frac{\partial^2 \bar{n}}{\partial \bar{r}^2} + \frac{\partial^2 \bar{n}}{\partial \bar{z}^2} + \frac{1}{\bar{r}} \frac{\partial \bar{n}}{\partial \bar{r}} \right]. \end{aligned} \tag{13}$$

Their respective boundary conditions become:

$$\begin{aligned} (\bar{u}(a(\bar{r}), \bar{z}, \bar{t}), \bar{w}(a(\bar{r}), \bar{z}, \bar{t})) &= \left( 0, \frac{4v\bar{z}}{1 - \beta\bar{t}} + N_1 v \frac{\partial \bar{w}}{\partial \bar{r}} \right) \text{ at} \\ \bar{r} &= a(\bar{r}), \end{aligned} \tag{14}$$

$$\begin{aligned} \bar{T} &= \bar{T}_\infty + \bar{D}_1 \frac{\partial \bar{T}}{\partial \bar{r}}, \quad D_B \frac{\partial \bar{C}}{\partial \bar{r}} + \frac{D_T}{T_\infty} \frac{\partial \bar{T}}{\partial \bar{r}} = 0, \quad \bar{n} = \bar{n}_w \text{ at} \\ \bar{r} &= a(\bar{r}). \end{aligned} \tag{15}$$

$$\begin{aligned} \bar{w} &= 0, \quad \bar{n} = 0, \quad \bar{T} = \bar{T}_\infty, \quad \bar{C} = \bar{C}_\infty \text{ at } \bar{r} \rightarrow \infty. \end{aligned} \tag{16}$$

In the above equations,  $\bar{T}_w$  is the surface temperature,  $N_1$  is the velocity slip parameter,  $\bar{n}_w$  is the surface density of motile-organism,  $\bar{k}_p$  Permeability of porous medium,  $c_F$  Forchheimer coefficient,  $Q_0$  represents the heat source when  $Q_0 > 0$  and the heat sink  $Q_0 < 0$  and  $\bar{D}_1$  is the thermal slip factor. Defining the following similarity transformation and dimensionless variables [44]

$$\begin{aligned} \xi &= \frac{\bar{r}^2}{a_0^2(1 - \beta\bar{t})}, \quad \bar{u} = -\frac{1}{a_0\sqrt{\xi}} \frac{2\nu F(\xi)}{\sqrt{1 - \beta\bar{t}}}, \\ \bar{w} &= \frac{4v\bar{z}}{a_0^2(1 - \beta\bar{t})} F'(\xi), \quad \theta(\xi) = \frac{\bar{T} - \bar{T}_\infty}{\bar{T}_w - \bar{T}_\infty}, \\ \phi &= \frac{\bar{C} - \bar{C}_\infty}{C_\infty}, \quad \Phi = \frac{\bar{n}}{\bar{n}_w}. \end{aligned} \tag{17}$$

and using Eq. (8) into Eqs. (1)–(7), we get

$$\begin{aligned} \xi F''' + (1 + F)F'' - F'^2 - S(\xi F'' + F') - MF' - k_f F'^2 \\ - kF' = 0, \end{aligned} \tag{18}$$

$$\begin{aligned} \xi \theta'' + \theta' + \frac{4\xi}{3} R_d \theta'' + \frac{2}{3} R_d \theta' + PrF\theta' - PrS\xi\theta' \\ + \xi \{ N_b \phi' \theta' + N_t \theta'^2 \} + H_s = 0, \end{aligned} \tag{19}$$

$$\begin{aligned} N_b \xi \phi'' + N_b \phi' + ScN_b \{ F\phi' - S\xi\phi' \} + N_t \{ \xi\theta'' + \theta' \} \\ - \gamma\phi = 0, \end{aligned} \tag{20}$$

$$\begin{aligned} \xi \Phi'' + \Phi' + Sb \{ F\Phi' - S\xi\Phi' \} \\ - P_e \left\{ \xi\Phi\phi'' + \frac{1}{2}\Phi\phi' + \xi\phi'\Phi' \right\} = 0. \end{aligned} \tag{21}$$

Their corresponding boundary conditions are

$$F(1) = F_w, F'(1) = 1 + \beta F''(1), \quad F'(\infty) = 0, \tag{22}$$

$$\theta(1) = 1 + \beta_T \theta'(1), \quad \theta(\infty) = 0, \tag{23}$$

$$N_b \phi'(1) + N_t \theta'(1) = 0, \quad \phi(\infty) = 0, \tag{24}$$

$$\Phi(1) = 1, \quad \Phi(\infty) = 0. \tag{25}$$

where

$$\begin{aligned} S &= \frac{\bar{\beta}a_0^2}{4\nu}, \quad N_b = \frac{\tau D_B \bar{C}_\infty}{\bar{\alpha}_m}, \quad N_t = \frac{\tau D_T [\bar{T}_w - \bar{T}_\infty]}{\bar{\alpha}_m}, \\ Sc &= \frac{\nu}{D_B}, \quad Sb = \frac{\nu}{D_{\bar{n}}}, \quad Pe = \frac{\bar{b}W_c}{D_{\bar{n}}}, \quad \beta = \frac{2[N_1]_0 \nu}{a_0}, \\ \beta_T &= \frac{2[\bar{D}_1]_0 \nu}{a_0}, \quad R_d = \frac{4\sigma \bar{T}^3}{k'\kappa}, \quad Pr = \frac{\nu}{\bar{\alpha}_m}, \\ M &= \frac{\sigma B_0^2}{4\nu\rho} [a_0^2(1 - \beta\bar{t})], \quad k = \frac{\mu}{\rho\nu k_p} [a_0^2(1 - \beta\bar{t})], \\ k_f &= \frac{\mu z}{\rho k_p^{1/2}}. \end{aligned} \tag{26}$$

In the above equations,  $S$  is the unsteady parameter,  $Pr$  is the Prandtl number,  $N_b$  Brownian motion coefficient,  $N_t$  thermophoresis coefficient,  $Sc$  is the Schmidt number,  $Sb$  bio-convection Schmidt number,  $Pe$  is the Peclet number,  $\beta$  is the velocity slip,  $k_f$  is Forchheimer number,  $\beta_T$  is the thermal slip,  $M$  is the magnetic parameter,  $R_d$  is a thermal radiation parameter,  $\gamma$  is the chemical reaction parameter,  $H_S$  is dimensionless heat source/sink parameter.

### 3 Physical quantities of interest

The physical quantities of interest such as skin friction coefficient, local Nusselt number, Sherwood number, local density number of motile microorganisms are defined as [44]

$$C_{F\bar{x}} = \frac{\tau_w}{\rho \bar{w}_w^2/2}, \quad Nu_{\bar{x}} = \frac{\bar{a}(\bar{r})q_w}{2k(\bar{T} - \bar{T}_\infty)},$$

$$Sh_{\bar{x}} = \frac{\bar{a}(\bar{r})q_M}{2D_B(\bar{C} - \bar{C}_\infty)}, \quad N_{n\bar{x}} = \frac{\bar{a}(\bar{r})q_N}{2k\bar{n}_w}. \tag{27}$$

where  $\tau_w$ ,  $q_w$ ,  $q_M$  and  $q_N$  are the shear stress, surface heat flux, surface mass flux and the motile surface microorganism flux which are defined as

$$\tau_w = \mu \left. \frac{\partial \bar{w}}{\partial \bar{r}} \right|_{\bar{r}=a(\bar{r})}, \quad q_w = -\kappa \left. \frac{\partial \bar{T}}{\partial \bar{r}} \right|_{\bar{r}=a(\bar{r})}, \quad q_M = -D_B \left. \frac{\partial \bar{C}}{\partial \bar{r}} \right|_{\bar{r}=a(\bar{r})},$$

$$q_N = \left. \frac{\partial \bar{n}}{\partial \bar{r}} \right|_{\bar{r}=a(\bar{r})}. \tag{28}$$

Using Eq. (17) and Eq. (27), we have

$$C_{F\bar{x}} = F''(1), \quad Nu_{\bar{x}} = -\left(1 + \frac{4}{3}R_d\right)\theta'(1),$$

$$Sh_{\bar{x}} = -\phi'(1), \quad N_{n\bar{x}} = -\Phi'(1). \tag{29}$$

### 4 Method of solution: shooting method

The exact solution for Eqs. (18) to (21) is not possible, for this purpose, we have employed shooting method to obtain the solution. Initially, all the equations are reduced to first-order differential equations and then shooting method is applied with a suitable initial guess. Equations (18) to (21) are reduced to the following form

$$F' = u_1, u_1' = u_2, u_2' = -\frac{1}{\xi}$$

$$[(1 + F)u_2 - u_1^2 - S(\xi u_2 + u_1) - Mu_1 - k_f u_1^2 - ku_1], \tag{30}$$

$$\theta' = v_1, v_1' = \frac{-1}{\xi(1 + \frac{4}{3}R_d)} \left[ v_1 + \frac{2}{3}R_d v_1 + PrFv_1 - PrS\xi v_1 \right.$$

$$\left. + \xi(N_b v_1 w_1 + N_t v_1^2) + H_S \right], \tag{31}$$

$$\phi' = w_1, w_1' = -\frac{1}{\xi N_b}$$

$$[N_b w_1 + ScN_b(Fw_1 - S\xi w_1) + N_t(\xi v_1' + v_1) - \gamma\phi], \tag{32}$$

$$\Phi' = r_1, r_1' = -\frac{1}{\xi}$$

$$\left[ r_1 + Sb(Fr_1 - S\xi r_1) - Pe \left( \xi \Phi w_1' + \frac{\Phi}{2} w_1 + \xi w_1 r_1 \right) \right], \tag{33}$$

and their corresponding boundary conditions reduces to the following form

$$F(1) = F_w, u_1(1) = 1 + \beta u_2(1), \quad u_2(1) = s_1. \tag{34}$$

$$\theta(1) = 1 + \beta_T v_1(1), \quad v_1(1) = s_2. \tag{35}$$

$$N_b w_1(1) + N_t v_1(1) = 0, \quad \phi(1) = s_3. \tag{36}$$

$$\Phi(1) = 0, \quad w_1(1) = s_4. \tag{37}$$

where  $s_1, s_2, s_3$  and  $s_4$  are the initial guess. ‘‘Matlab’’ is used for numerical computations of shooting technique with error less than  $10^{-4}$ , while the step is taken  $\Delta\xi = 1 \times 10^{-4}$ .

### 5 Numerical results and discussion

This section deals with graphical and numerical results of all the governing parameters arises in the governing flow problem. Particularly, we discussed the effects of Forchheimer number  $k_f$ , porosity parameter  $k$ , magnetic parameter  $M$ , Brownian motion parameter  $N_b$ , thermophoresis parameter  $N_t$ , chemical reaction parameter  $\gamma$ , unsteady parameter  $S$ , Schmidt number  $Sc$ , Peclet number  $Pe$ , heat source/sink parameter  $H_S$ , radiation parameter  $R_d$ , velocity slip  $\beta$ , thermal slip  $\beta_T$ , Prandtl number  $Pr$  and bio-convection Schmidt number  $Sb$  on velocity  $F'$ , temperature  $\theta$ , nanoparticle concentration  $\phi$  and motile microorganism density  $\Phi$  profile. Table 1 shows the numerical comparison with the exiting published results [42–44] as a special case of our study by taking  $M = \gamma = R_d = k_f = k = H_S = 0$ . The numerical comparison shows that the present results are in excellent agreement which also confirms the validity of the present methodology. All the numerical computations have been carried out for the following parametric values:  $k = 1, N_b = 0.1, N_t = 0.1, \gamma = 1, Sb = 10, M = 2, Pe = 0.1, Sc = 10, \beta = 0.1, \beta_T = 0.1, k_f = 3, H_S = 0.1, S = 0.1, Pr = 6.8$ . Numerical values of local Nusselt number, skin friction coefficient, local Sherwood number and motile microorganism of local density are presented in Table 2 against all the emerging parameters.

Figures 2a, b and 3a, b are sketched for velocity against all the involved parameters. It depicts from Fig. 2a the

**Table 1** Numerical comparison for skin friction coefficient and local Nusselt number by taking  $M = \gamma = R_d = k_f = k = H_S = 0$

	Ishak et al. [42]	Wang [43]	Md Faisal Md Bashir [44]	Present results
$F''(1)$	-1.1780	-1.1777	-1.1780	-1.1780
$-\theta'(1)$	2.0587	2.059	2.0586	2.0586

**Table 2** Numerical values of Nusselt number, Sherwood number, skin friction coefficient and motile microorganism of local density number

$M$	$S$	$R_d$	$N_b$	$N_t$	$\gamma$	$Sb$	$Sc$	$Pe$	$k_f$	$k$	$H_S$	$C_{F\bar{x}}$	$Nu_{\bar{x}}$	$Sh_{\bar{x}}$	$N_{n\bar{x}}$
0	-0.1	1	0.1	0.1	1	10	10	0.1	0	0	0	-1.3815	5.4282	19.4053	6.9082
	0											-1.3513	4.9505	15.6200	5.9316
	0.1											-1.3229	4.4470	12.3226	4.9497
2	-0.1											-1.8311	5.4283	19.6243	6.8158
	0											-1.8022	4.9507	15.6892	5.8203
	0.1											-1.7743	4.4471	12.1632	4.8103
		2										-1.7743	5.0021	12.2973	4.8633
		3										-1.7743	5.6452	8.16934	4.8862
			0.2									-1.7743	4.4474	13.2081	4.9032
			0.3									-1.7743	4.4474	13.9204	4.9342
				0.2								-1.7743	4.4097	12.2377	4.6279
				0.3								-1.7743	4.3723	12.1593	4.4485
					2							-1.7743	4.4460	12.1632	4.8102
					3							-1.7743	4.4448	12.1632	4.8101
						11						-1.7743	4.4471	12.3226	5.2443
						15						-1.7743	4.4471	12.3226	6.9548
							20					-1.7743	4.4389	21.7782	4.8098
							30					-1.7743	4.4346	32.2966	4.8094
								0.5				-1.7743	4.4346	12.1632	4.0682
								1				-1.7743	4.4471	12.1632	3.1422
									1			-1.8653	4.5393	12.1632	4.7816
									3			-2.0229	4.5393	12.1632	4.7388
										0.5		-2.0924	4.5394	12.5004	4.7163
										1		-2.1579	4.5394	12.4980	4.6951
											-0.2	-2.1579	4.5932	12.6158	4.6928
											0.2	-2.1579	4.4840	12.3768	4.6974

greater influence of magnetic field causes a reduction in the velocity profile. Physically, when an external magnetic field is applied to any electrically conducting fluid, then a repulsive force originated known as “Lorentz force” which tends to oppose the flow markedly. It can also be seen from this figure that unsteady parameter is favourable to enhance the velocity of the fluid. It is worth mentioning here that positive values of  $S > 0$  are associated with accelerating flow and negative values of  $S < 0$  are associated with decelerating flow across the surface of the stretching cylinder. Moreover, for  $S = 0$  corresponds to steady state problem, while  $S \neq 0$  correspond to unsteady. It can be observed from Fig. 2b that Forchheimer parameter also opposes the flow substantially, while the variation in velocity becomes smaller as the effects of magnetic field increase. Furthermore, we can also notice from Fig. 3a that

porosity parameter causes a significant reduction in the velocity profile. The effects of porosity are modelled as  $-kF' - k_f F'^2$  [see Eq. (18)] which also contains a strong nonlinear term  $F'^2$ . With progressively larger porosity, the matrix resistance produced due to solid fibres towards a porous medium is energised and hence the porous drag force increases, resulting that fluid decelerate very significantly. Figure 3b shows the variation of velocity against slip parameter  $\beta$ . It depicts from this figure that an increment in slip parameter  $\beta$  causes a markedly decline the velocity of the fluid. Physically, when the slip effect ensues, the drag force on the stretching wall is partially transferred to the fluid and hence the velocity of the fluid depleted. Moreover, with an increment in a hydrodynamic slip parameter tends to reduce the magnitude of a wall shear stress.

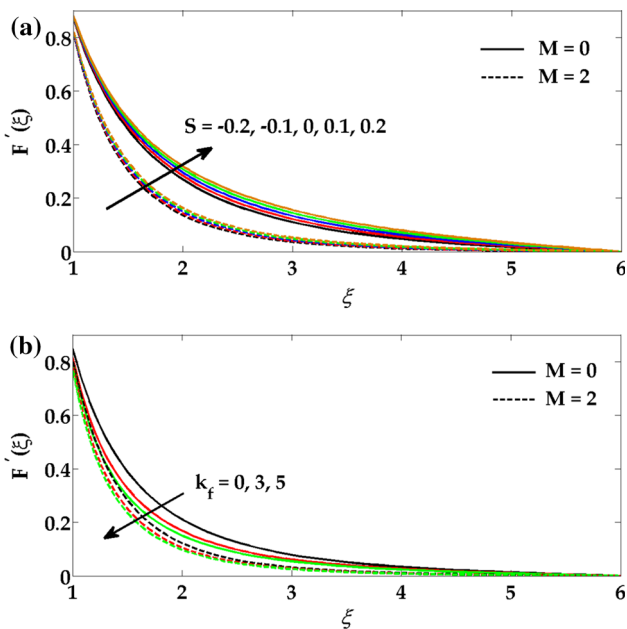


**Fig. 2** Effect of magnetic parameter  $M$  and unsteady parameter  $S$ , Forchheimer number  $k_f$  and magnetic parameter  $M$  on velocity profile

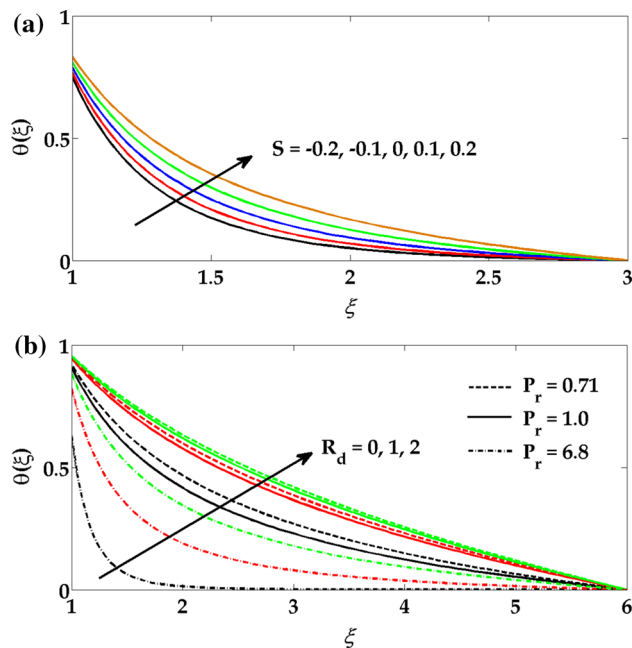


**Fig. 4** Effect of unsteady parameter  $S$ , radiation parameter  $R_d$  and Prandtl number  $Pr$  on temperature profile

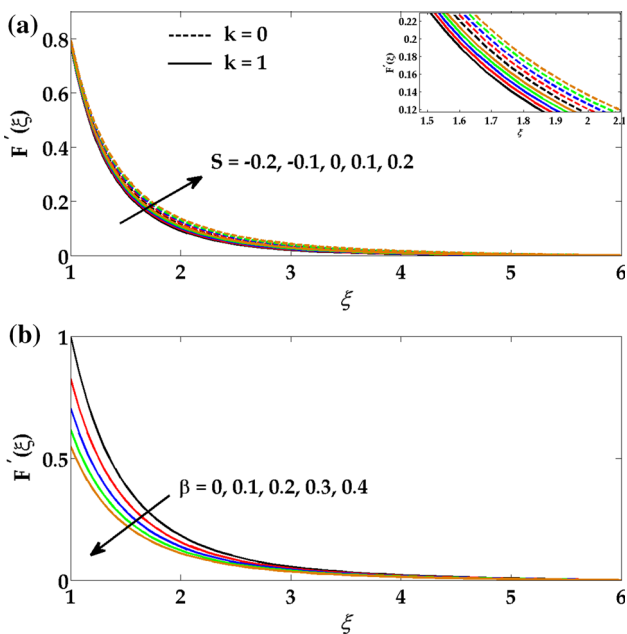


**Fig. 3** Effect of unsteady parameter  $S$  and porosity parameter  $k$  and slip parameter  $\beta$  on velocity profile

Figures 4a, b, 5 and 6 are sketched for temperature profile against unsteady parameter  $S$ , radiation parameter  $R_d$ , Prandtl number  $Pr$ , heat source/sink parameter  $H_S$ , thermophoresis parameter  $N_t$  and thermal slip parameter  $\beta_T$ . It depicts from Fig. 4a that for higher values of unsteady parameter  $S$ , the temperature profile rises very significantly. From Fig. 4b we can see that higher values of radiation parameter  $R_d$  enhance the temperature profile and

its boundary layer thickness. Physically, for higher values of radiation parameter  $R_d$  gives more heat to the governing fluid that reveals an increment in its boundary layer thickness and temperature profile. Furthermore, we can also see that higher values of Prandtl number  $Pr$  cause a significant reduction in temperature profile and its relevant boundary layer thickness. Large values of Prandtl number  $Pr$  are associated with weaker thermal diffusivity. Those fluids that contain weaker thermal diffusivity have a lower temperature. Such kind of weaker thermal diffusivity reveals a decrement in the temperature profile and its boundary layer thickness. It depicts from Fig. 5a that thermophoresis parameter also enhances the temperature profile markedly. An enhancement in thermophoresis parameter  $N_t$  produced thermophoresis forces which allow moving the nanoparticles from hotter area to colder region and as a result, it tends to rise the thermal boundary layer thickness and temperature profile. It can be observed from Fig. 5b that heat source/sink parameter  $H_S$  enhances the temperature profile and its corresponding boundary layer thickness. It can be scrutinised from Fig. 6 that an increment in thermal slip parameter  $\beta_T$  causes a compelling reduction in the temperature profile. Physically, when the thermal slip parameter increases, then the movement of the fluid within a boundary layer will not be very sensitive due to the heating influence of cylindrical surface. A reduction in a temperature (thermal energy) profile will be transferred from a hot cylinder to the fluid, and as a result a reduction in the temperature profile has been observed, i.e. a



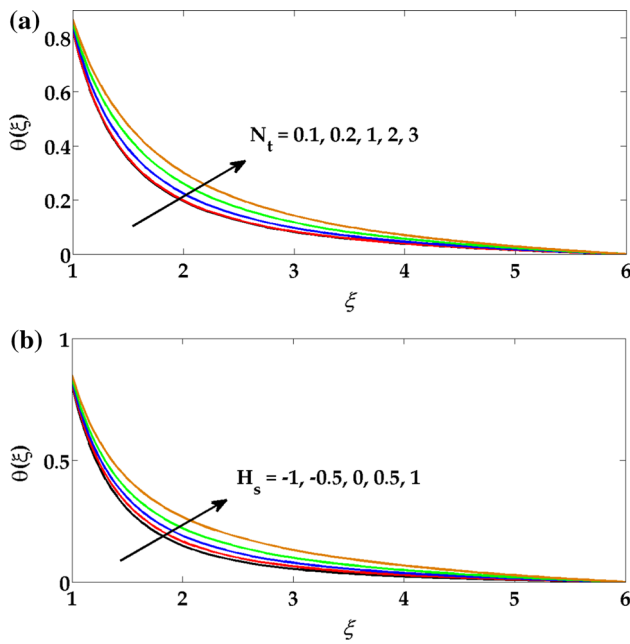


**Fig. 5** Effect of thermophoresis parameter  $N_t$  and heat source/sink parameter  $H_s$  on temperature profile

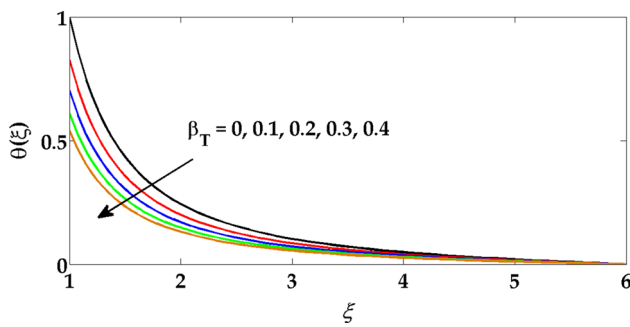


**Fig. 6** Effect of thermal slip  $\beta_T$  on temperature profile

decrement in a thermal boundary layer thickness (thinning and cooling of thermal boundary layer).

Figures 7a, b and 8 show the effects of unsteady parameter  $S$ , Brownian motion parameter  $N_b$ , thermophoresis parameter  $N_t$ , chemical reaction parameter  $\gamma$  and Schmidt number  $Sc$  on nanoparticle concentration profile. It depicts from Fig. 7a that when the unsteady parameter  $S$  increases then the nanoparticle concentration profile and its boundary layer thickness increases. It can be examined from Fig. 7b that for large values of Brownian motion parameter  $N_b$ , nanoparticle concentration profile decreases substantially. The presence of nanoparticles in the nanofluid, the Brownian motion takes place with the rise of Brownian motion parameter  $N_b$  and as a result the nanoparticle concentration profile and its corresponding boundary layer thickness diminish. Furthermore, we can also see that the greater influence of thermophoresis parameter  $N_t$  also enhances the boundary layer thickness

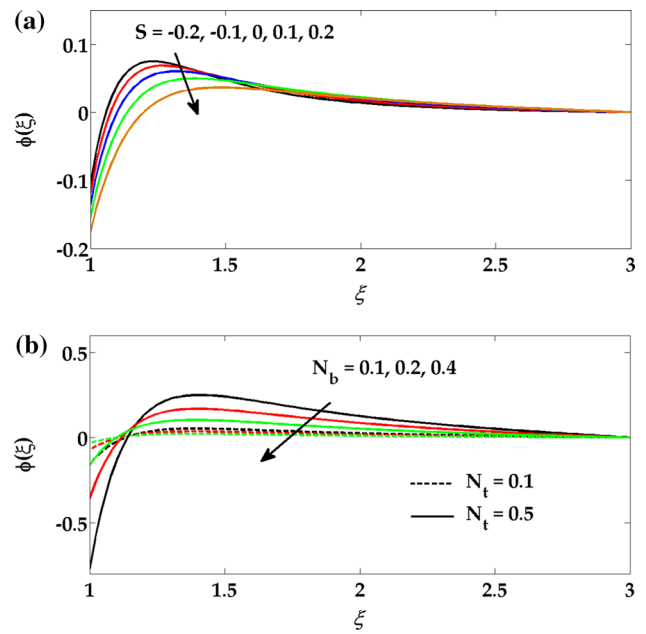


**Fig. 7** Effect of unsteady parameter  $S$ , thermophoresis parameter  $N_t$  and Brownian motion parameter  $N_b$  on concentration profile

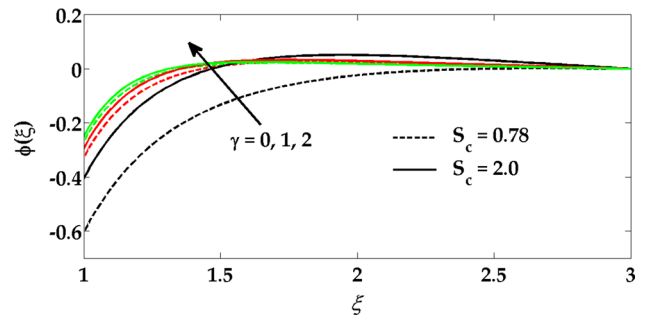


**Fig. 8** Effect of chemical reaction parameter  $\gamma$  and Schmidt number  $Sc$  on concentration profile

and nanoparticle concentration profile. From Fig. 8 we can see that concentration profile increases significantly for large values of chemical reaction parameter  $\gamma$ . Moreover, we can also notice that Schmidt number  $Sc$  also enhances strongly the nanoparticle concentration profile and its boundary layer thickness. Figure 9a, b is sketched for motile microorganism density against bio-convection Schmidt number  $Sb$ , unsteady parameter  $S$  and Peclet number  $Pe$ . It depicts from Fig. 9a that bio-convection Schmidt number  $S_b \left( = \frac{\nu}{D_b} \right)$  tends to diminish the microorganism density profile. This parameter is solely arises in the microorganism density profile [see Eq. (21)] and is defined as the ratio of a momentum diffusivity and microorganism diffusivity. An increment in bio-convection Schmidt number causes a diffusivity difference to rise and a rate of momentum diffusion controls the microorganism

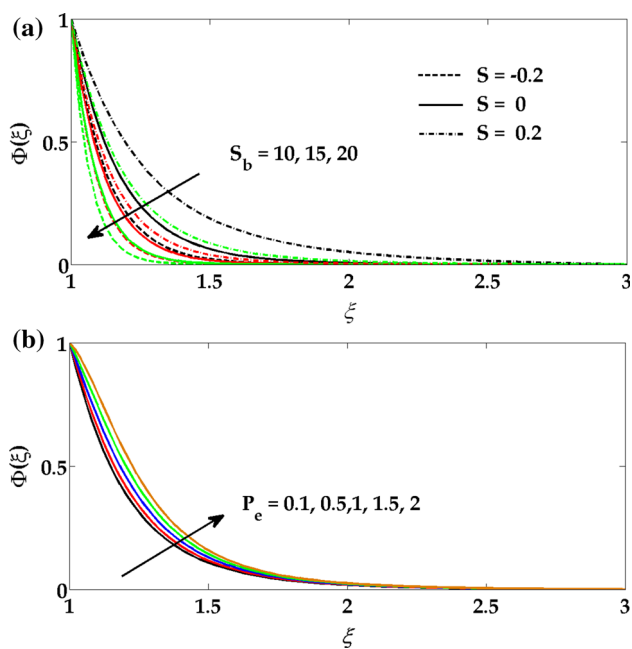


**Fig. 9** Effect of Peclet number  $Pe$ , bio-convection Schmidt number  $S_b$  and unsteady parameter  $S$  on motile microorganism density profiles

diffusion rate and as a result a reduction in the microorganism density profile has been observed (see Fig. 9a). It can also be seen in Fig. 9a that for  $S > 0$  (accelerating flow) the microorganism density profile is higher as compared to the decelerating flow  $S < 0$ . It can be notice from Fig. 9b that microorganism density profile is strongly increased for large values of Peclet number  $Pe$ .  $Pe \left( = \frac{\bar{b}W_c}{D_{\bar{n}}} \right)$  is directly proportional to  $W_c$  (maximum speed of cell swimming) and  $\bar{b}$  (chemotaxis constant), whereas it is inversely proportional to diffusivity of microorganism  $D_{\bar{n}}$ . Hence large values of Peclet number will reduce the diffusivity of microorganism and/or microorganism speed will

be diminished. As a result, the microorganism density profile and its associated boundary layer thickness increase as shown in Fig. 9b. The present study reveals various interesting behaviour that warrant further study on nano-fluid having gyrotactic microorganism. Figures 10, 11, 12 and 13 are plotted for skin friction coefficient, motile microorganism density number, Nusselt number and Sherwood number versus magnetic parameter for multiple values of suction/injection parameter  $F_w$ .

## 6 Conclusion

In this article, three-dimensional MHD nanofluid boundary layer flow having gyrotactic microorganism through a porous stretching cylinder has been examined. The effects of thermal radiation, chemical reaction, velocity slip and thermal slip are also taken into account. Similarity transformation variables are used to model the governing equations. The resulting highly nonlinear coupled partial differential equations are solved numerically with the help of shooting method. The influence of all the emerging parameters is discussed with the help of graphs and tables. Comparison with the existing published results is also presented as a special case of our study. The major points for the present study are summarised below:

1. Magnetic and porosity effects cause a reduction in the velocity profile.
2. The influence of slip parameter shows a significant increase in the velocity profile.
3. Radiation parameter tends to rise the temperature profile and its boundary layer thickness, while Prandtl number and thermal slip show opposite behaviour.
4. Brownian motion thermophoresis parameter shows converse behaviour on concentration profile.

**Fig. 10** Skin friction coefficient versus magnetic parameter  $M$

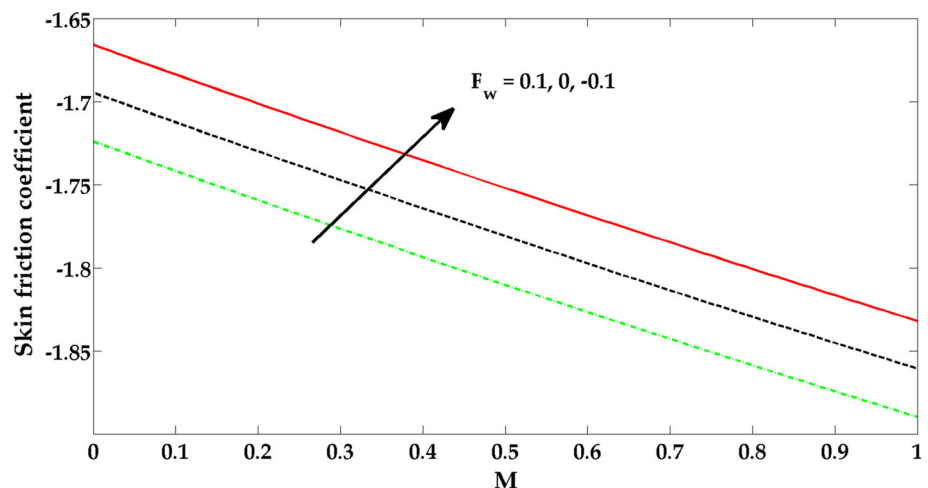


**Fig. 11** Nusselt number versus magnetic parameter  $M$

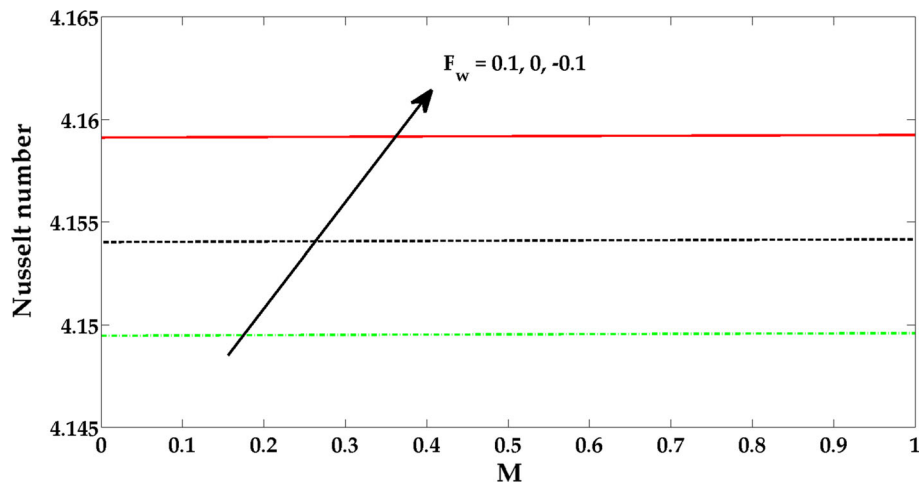


**Fig. 12** Sherwood number versus magnetic parameter  $M$

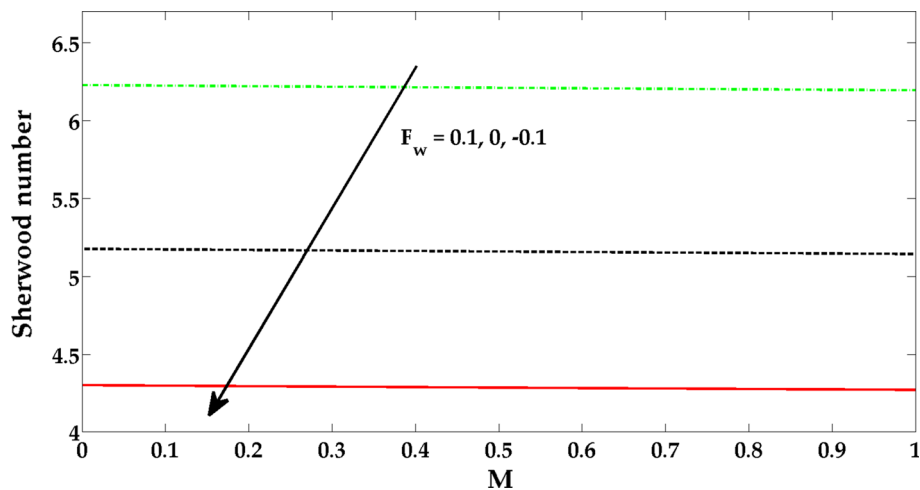
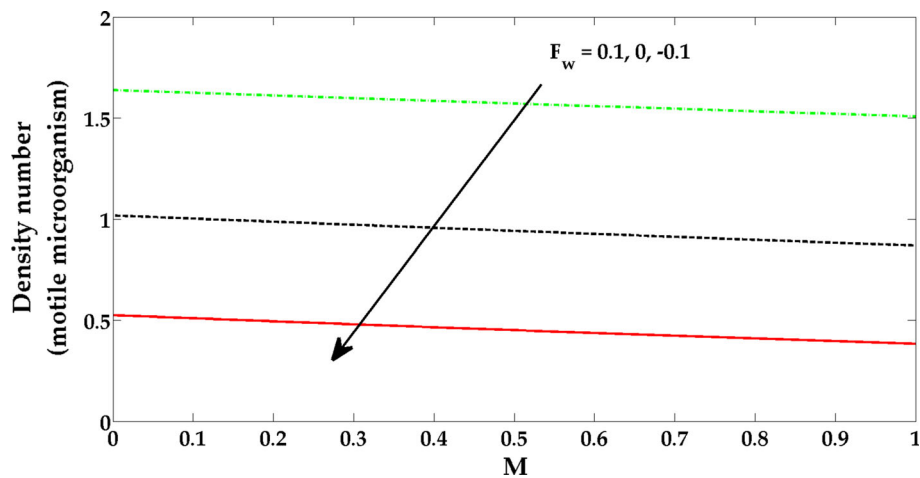


**Fig. 13** Density number (motile microorganism) versus magnetic parameter  $M$



5. Chemical reaction parameter and Schmidt number markedly enhance the concentration profile.
6. Heat source/sink parameter tends to rise the temperature profile significantly.
7. Peclet number enhances the motile microorganism density profile, while bio-convection Schmidt number depicts opposite behaviour.

The present study reveals various interesting behaviour that warrants further study on nanofluid having gyrotactic microorganism.

#### Compliance with ethical standards

**Conflict of interest** The authors declare no conflict of interest.

## References

1. Thomas S, Yang W (eds) (2009) *Advances in polymer processing: from macro-to nano-scales*. Woodhead Publishing, Oxford
2. Bachok N, Ishak A (2010) Flow and heat transfer over a stretching cylinder with prescribed surface heat flux. *Malays J Math Sci* 4:159–169
3. Stasiak J, Squires AM, Castelletto V, Hamley IW, Moggridge GD (2009) Effect of stretching on the structure of cylinder and sphere-forming styrene–isoprene–styrene block copolymers. *Macromolecules* 42:5256–5265
4. Sakiadis BC (1961) Boundary layer behaviour on continuous solid surfaces: I. Boundary layer equations for two-dimensional and axisymmetric flow. *AIChE J* 7:26–28
5. Crane LJ (1970) Flow past a stretching plate. *Z Angew Math Phys* 21(4):645–647. doi:10.1007/BF01587695
6. Datta BK, Roy P, Gupta AS (1985) Temperature field over a stretching sheet with uniform heat flux. *Int J Heat Mass Transf* 12:89–94
7. Chen CK, Char MI (1988) Heat transfer of a continuous stretching surface with suction and blowing. *J Math Anal Appl* 135:568–580
8. Bhatti MM, Shahid A, Rashidi MM (2016) Numerical simulation of fluid flow over a shrinking porous sheet by successive linearization method. *Alex Eng J* 55:51–56
9. Bhatti MM, Abbas T, Rashidi MM (2016) A New numerical simulation of MHD stagnation-point flow over a permeable stretching/shrinking sheet in porous media with heat transfer. *Iran J Sci Technol Trans A Sci*. doi:10.1007/s40995-016-0027-6
10. Saidur R, Leong KY, Mohammad HA (2011) A review on applications and challenges of nanofluids. *Renew sustain Energy Rev* 15:1646–1668
11. Wong KV, De Leon O (2010) Applications of nanofluids: current and future. *Adv Mech Eng* 2:519659
12. Yu W, Xie H (2012) A review on nanofluids: preparation, stability mechanisms, and applications. *J Nanomater* 2012:1
13. Raees A, Xu H, Liao SJ (2015) Unsteady mixed nano-bioconvection flow in a horizontal channel with its upper plate expanding or contracting. *Int J Heat Mass Transf* 86:174–182
14. Anoop KB, Sundararajan T, Das SK (2009) Effect of particle size on the convective heat transfer in nanofluid in the developing region. *Int J Heat Mass Transf* 52:2189–2195
15. Pedley TJ (2010) Instability of uniform micro-organism suspensions revisited. *J Fluid Mech* 647:335–359
16. Xu H, Pop I (2014) Mixed convection flow of a nanofluid over a stretching surface with uniform free stream in the presence of both nanoparticles and gyrotactic microorganisms. *Int J Heat Mass Transf* 75:610–623
17. Aziz A, Khan WA, Pop I (2012) Free convection boundary layer flow past a horizontal flat plate embedded in porous medium filled by nanofluid containing gyrotactic microorganisms. *Int J Therm Sci* 56:48–57
18. Tham L, Nazar R, Pop I (2013) Mixed convection flow over a solid sphere embedded in a porous medium filled by a nanofluid containing gyrotactic microorganisms. *Int J Heat Mass Transf* 62:647–660
19. Saranya S, Radha KV (2014) Review of nanobiopolymers for controlled drug delivery. *Polym Plast Technol Eng* 53:1636–1646
20. Oh JK, Lee DI, Park JM (2009) Biopolymer-based microgels/nanogels for drug delivery applications. *Prog Polym Sci* 34:1261–1282
21. Abo-Eldahab EM, Abd El-Aziz M (2000) Radiation effect on heat transfer in electrically conducting fluid at a stretching surface with uniform free stream. *J Phys D Appl Phys* 33:3180–3185
22. Cortell R (2008) Effects of viscous dissipation and radiation on the thermal boundary layer over a nonlinearly stretching sheet. *Phys Lett A* 372:631–636
23. Cortell R (2006) Effects of viscous dissipation and work done by deformation on MHD flow and heat transfer of a viscoelastic fluid over a stretching sheet. *Phys Lett A* 357:298–305
24. Bhatti MM, Abbas T, Rashidi MM, Ali MES (2016) Numerical simulation of entropy generation with thermal radiation on MHD carreau nanofluid towards a shrinking sheet. *Entropy* 18(6):200
25. Bhatti MM, Rashidi MM (2016) Effects of thermo-diffusion and thermal radiation on Williamson nanofluid over a porous shrinking/stretching sheet. *J Mol Liq* 221:567–573
26. Bhatti MM, Rashidi MM (2016) Entropy generation with non-linear thermal radiation in MHD boundary layer flow over a permeable shrinking/stretching sheet: numerical solution. *J Nanofluids* 5:543–548
27. Anjalidevi SP, Kandasamy R (1999) Effects of chemical reaction, heat and mass transfer on laminar flow along a semi infinite horizontal plate. *Heat Mass Transf* 35:465–467
28. Hayat T, Muhammad T, Shehzad AS, Alsaedi A (2015) Similarity solution to threedimensional boundary layer flow of second grade nanofluid past a stretching surface with thermal radiation and heat source/sink. *AIP Adv* 5:017107
29. Abel MS, Siddheshwar PG, Mahesha N (2009) Effects of thermal buoyancy and variable thermal conductivity on the MHD flow and heat transfer in a power-law fluid past a vertical stretching sheet in the presence of a non-uniform heat source. *Int J Non Linear Mech* 44:1–12
30. Sheikholeslami M, Rashidi MM (2015) Effect of space dependent magnetic field on free convection of  $Fe_3O_4$ -water nanofluid. *J Taiwan Inst Chem Eng*. doi:10.1016/j.jtice.2015.03.035
31. Sheikholeslami M (2014) Effect of spatially variable magnetic field on ferrofluid flow and heat transfer considering constant heat flux boundary condition. *Eur Phys J Plus* 2014:129–248
32. Sheikholeslami M, Ganji DD, Rashidi MM (2015) Ferrofluid flow and heat transfer in a semi annulus enclosure in the presence of magnetic source considering thermal radiation. *J Taiwan Inst Chem Eng* 47:6–17
33. Ishak A, Nazar R, Pop I (2008) Magnetohydrodynamics flow and heat transfer due to a stretching cylinder. *Energy Convers Manag* 49:3265–3269
34. Mukhopadhyay S (2013) MHD boundary layer slip flow along a stretching cylinder. *Ain Shams Eng J* 4:317–324
35. Ishak A (2010) Unsteady MHD flow and heat transfer over a stretching plate. *J Appl Sci* 10:2127–2131
36. Pop I, Na TY (1998) A note on MHD flow over a stretching permeable surface. *Mech Res Commun* 25:263–269

37. Khan K, Abel MS, Sonth RM (2003) Visco-elastic MHD flow heat and mass transfer over a porous stretching sheet with dissipation of energy and stress work. *Heat Mass Trans* 40:47–57
38. Abed Mahdi R, Mohammed HA, Munisamy KM, Saeid NH (2015) Review of convection heat transfer and fluid flow in porous media with nanofluid. *Renew Sust Energy Rev* 41:715–734
39. Abed Mahdi R, Mohammed HA, Munisamy KM (2013) Improvement of convection heat transfer by using porous media and nanofluid: review. *Int J Sci Res* 2:34–47
40. Das KS, Choi SU, Yu W, Pradeep T (2007) *Nanofluid: science and technology*. Wiley, London
41. James M, Mureithi EW, Kuznetsov D (2014) Natural convection flow past an impermeable vertical plate embedded in nanofluid saturated porous medium with temperature dependent viscosity. *Asian J Math Appl* 2014:ama0165
42. Ishak A, Nazar R, Pop I (2008) Magnetohydrodynamic (MHD) flow and heat transfer due to a stretching cylinder. *Energy Convers Manag* 49:3265–3269
43. Wang CY (1988) Fluid flow due to a stretching cylinder. *Phys Fluids* 31:466–468
44. Basir MFM, Uddin MJ, Ismail AM, Bég OA (2016) Nanofluid slip flow over a stretching cylinder with Schmidt and Péclet number effects. *AIP Adv* 6:055316